

Rare-gas thermal desorption from flat and stepped platinum surfaces: Lateral interactions and the influence of dimensionality

W. Widdra,* P. Trischberger, W. Frieß, and D. Menzel

Physik-Department E 20, Technische Universität München, D-85747 Garching, Germany

S. H. Payne and H. J. Kreuzer

Physics Department, Dalhousie University, Halifax, Nova Scotia, Canada B3H 3J5

(Received 26 August 1997)

High-resolution thermal-desorption data are presented for xenon desorption from flat Pt(111) and stepped Pt(997) surfaces. Analysis of the experimental data and comparison with detailed lattice-gas models which are able to describe different adsorption sites on the stepped surface reveal similar xenon single-particle binding energies of 253 meV and 264 meV on Pt(111) and on the terraces of a Pt(997) surface, respectively. The extracted corresponding lateral interactions are attractive and again of similar value (pairwise attraction of 11 meV). However, for terrace desorption different kinetics are observed: On the flat (111) surface desorption is zero order over a wide range of coverage, due to equilibrium between adsorbate condensate and two-dimensional gas, whereas on the stepped surface terrace desorption is near first order. We interpret the changed desorption kinetics as a consequence of the finite size of the (111) terraces in one direction on the stepped surface, i.e., as an influence of dimensionality on adlayer statistics. On the basis of the lattice-gas model we demonstrate the influence of different terrace widths. For adsorption on Pt(997) we find complete xenon step decoration before terrace adsorption starts with a binding energy of about 400 meV and a pairwise repulsion of about 16 meV. Completion of the step decoration is accompanied by a work function change of 0.47 eV which might explain the observed repulsion as due to dipole-dipole interaction along the steps.

[S0163-1829(98)03407-9]

I. INTRODUCTION

The experimental study of adsorption and desorption on atomically well-defined surfaces is always complicated at very low coverage by the unavoidable presence of defects such as steps and kinks. The latter are, however, of great interest due to their relevance for many catalytic processes as well as for epitaxial growth. This has led to efforts to study adsorption, desorption, and also simple reactions on faceted and stepped surfaces.¹ From a fundamental point of view adsorbate layers exhibit strictly two-dimensional (2D) behavior in many respects. Additional structuring of the substrate, e.g., by introduction of regular steps, can lead to further reduced dimensionality of the adsorbate system which might alter its structural, electronic, or thermodynamic properties. This is to be expected for selective adsorption at step sites, but also the finite size of the terraces between the steps may alter the properties of the adsorbate system.²

In this paper we will present a study of the desorption kinetics of xenon from Pt(997) and compare it to desorption from Pt(111). Rare gases are perceived to be simple model systems for atomic adsorption because of their weak interaction with the substrate except that the relatively strong lateral attraction in the adsorbate, often stronger than the adatom-surface potential corrugation depth, produces a series of interesting ordered phases that complicate the desorption kinetics as well.

In the temperature range 62–98 K xenon adsorbed on Pt(111) forms islands with a $(\sqrt{3} \times \sqrt{3})R30^\circ$ structure for coverages (relative to the number of Pt surface atoms) up to 0.33. Around 98 K a first-order 2D solid-liquid phase (actu-

ally solid plus gas to liquid plus gas) transition occurs as seen by the disappearance of any overlayer low-energy electron diffraction (LEED) pattern and by intensity changes in He-scattering.³ At higher coverages and temperatures below 81 K, the commensurate structure undergoes a continuous phase transition to a uniaxially compressed, striped incommensurate phase.⁴ Further compression at higher coverages leads to rotated hexagonal higher-order commensurate structures which finally, at a saturation coverage of 0.41, have a Xe-Xe spacing of 4.34 Å and a hexagonal rotation of 3.3° relative to $(\sqrt{3} \times \sqrt{3})R30^\circ$.^{5,6} Compared to this detailed information about the adsorbate structure on the flat (111) surface not much is known about the structure of xenon adlayers on stepped surfaces.

The adsorption at the step sites has attracted attention since these sites provide stronger substrate interactions as seen, for instance, as an additional high-temperature peak in temperature programmed desorption from nominally flat surfaces. The best Pt(111) surfaces still have a density of atomic steps of a fraction of 1% implying terrace widths on the order of 300 Å. In low-temperature scanning tunnel microscopy (STM) it has been seen that these sites are preferentially occupied even at the lowest adsorption temperature (4 K). This is most likely due to field-induced diffusion from the tip because thermally activated diffusion is negligible on the time scale of the experiment.⁷ The Pt(997) surface which consists nominally of 20.2-Å- (8.5 Pt-Pt rows) wide (111) terraces separated by monatomic steps exposing $(1\bar{1}1)$ microfacets (see Fig. 1) shows a regular terrace-step configuration with a narrow terrace width distribution.⁸ Xenon adsorp-

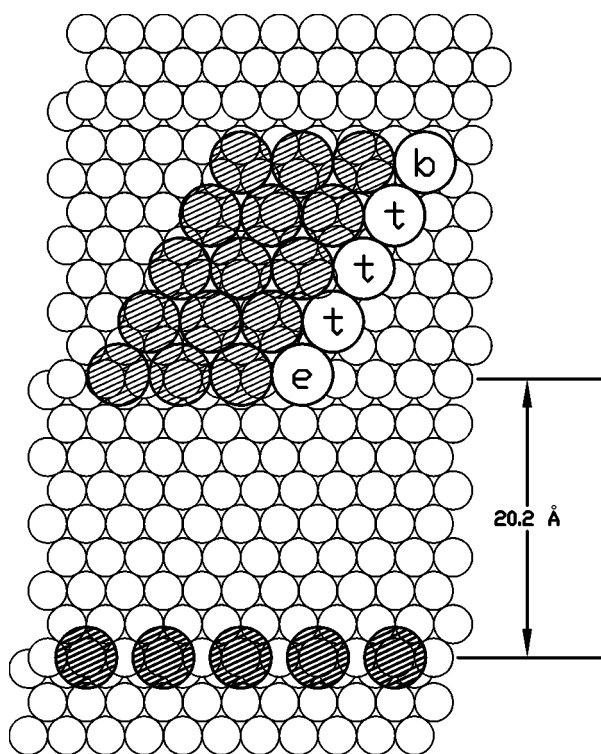


FIG. 1. A schematic view of the Pt(997) surface. Possible xenon structures which are compatible with the observed LEED patterns for xenon saturation and step decoration are indicated in the upper and lower part, respectively (the sites are chosen arbitrarily).

tion on this surface at 40 K leads to a line-by-line growth for the first two lines as seen by He scattering.⁹ This indicates again preferred adsorption at the step sites as also seen in STM.^{10,11}

The thermal desorption of xenon on Pt(111) has been studied extensively by Rettner, Bethune, and Schweizer¹² by a combination of molecular beam techniques. For low xenon coverages, they found Arrhenius behavior of the desorption rates over seven orders of magnitude, and derived an adsorption energy of 245 meV after saturation of defects (step sites) with CO. In the absence of defect passivation they found an initial adsorption energy of 410 meV which they attributed to adsorption at step edges. These results can be compared with the earlier results of 277 meV by Poelsema, Verheij, and Comsa,¹³ 239 meV by Wandelt, Hulse, and Küppers,¹⁴ and 330 meV by Nieuwenhuysh, Meijer, and Sachtler.¹⁵ As Rettner, Bethune, and Schweizer¹² have shown, defects may influence desorption data significantly. The influence of steps was investigated by Siddiqui *et al.* by comparison of thermal desorption from Pt(111), Pt(112), and Pt(557) surfaces.¹⁶ On the close-packed (111) surface they found ($T_{\text{ads}}=87$ K, non-linear heating) a desorption maximum at 93 K upshifting with increasing coverage, indicating an attractive lateral Xe-Xe interaction on the flat platinum terrace. On the stepped surfaces [(100) microfacets] they found an additional high-temperature desorption peak with an adsorption energy of about 370 meV, downshifting with coverage.¹⁶ This shift was interpreted as due to repulsive Xe-Xe interactions.

In this detailed study of xenon thermal desorption from flat Pt(111) as well as from stepped Pt(997) surfaces we compare high-resolution temperature programmed desorp-

tion (TPD) spectra with lattice-gas models which include different energetics for terrace and step sites as well as different lateral interactions between xenon atoms. As we will show by comparison of both surfaces, xenon adsorption and desorption on the (111) terraces of Pt(997) are both influenced by the steps, despite the rather wide terrace width of 20.2 Å.

II. EXPERIMENTAL DETAILS

The experiments were performed in two different UHV systems with base pressures below 10^{-10} mbar, each housing four grid LEED optics and a quadrupole mass spectrometer equipped with a Feulner cap to increase the dynamical range and resolution of desorption spectra.¹⁷ Using a liquid He cryostat, the samples could be cooled to 20 and 5 K, respectively, and resistively heated to 1300 K. The sample temperature measured by a chromel-alumel thermocouple was calibrated via desorption of the rare-gas multilayers, argon and xenon.¹⁸ The samples were cleaned by repeated cycles of 700-eV Ar⁺-ion bombardment at 800 K followed by annealing to 1200 K and repeated oxygen adsorption and desorption cycles. The carbon contamination was quantitatively determined via its oxidation products CO and CO₂ to be below 0.002 monolayers.

The techniques which serve to attain TPD spectra of physisorbed species with high resolution and precision, and over wide ranges, have been described before.¹⁸ They make it possible to attain five orders of magnitude in coverage and desorption rate, and to quantitatively calibrate both; and to use widely variable heating rates. Particular care has been taken to minimize the temperature gradients over the measurement area on the crystal in order to optimize the resolution of the spectra. The reproducibility of measurement is such that, e.g., a common leading edge for zero order of desorption is reproduced within the linewidth of the plot over wide ranges of coverage, so that deviations are very significant [see Fig. 2(b) below]. The mentioned temperature calibration assures the absolute values of energies to be correct. For further details see Ref. 19. Possible temperature gradients across the surface during thermal desorption are estimated to be below 1 K for the presented data.

III. EXPERIMENTAL RESULTS

A. Xe/Pt(111)

Xenon thermal desorption data from a nominally flat Pt(111) surface are shown on linear and logarithmic (Arrhenius) scales in Figs. 2(a) and 2(b), respectively. With increasing coverage the dominant high-temperature desorption peak shifts up from about 100 to 107 K and the desorption rate displays a common leading desorption edge over several orders of magnitude of rate for coverages between 0.03 and 0.33. This zero-order kinetics is indicative of desorption from the coexistence region of a 2D gas-condensate equilibrium within the xenon adlayer.²⁰ For coverages above 0.33, the coverage of the ordered $(\sqrt{3} \times \sqrt{3})R30^\circ$ structure for which xenon is adsorbed in threefold hollow sites,²¹ there is a small desorption peak at 95 K which is highly sensitive to the crystal quality. It is associated with the phase transition from a compressed phase to the ordered $\sqrt{3}$ layer when the coverage decreases by desorption. Similar behavior has been

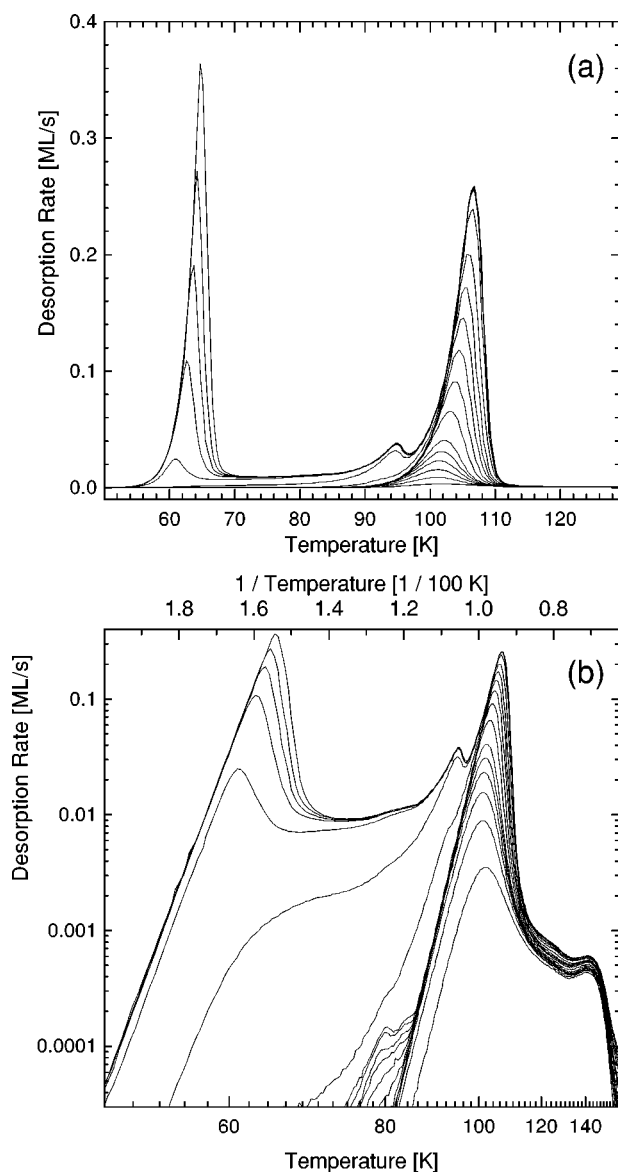


FIG. 2. Experimental TPD spectra for different xenon coverages on Pt(111) in the range up to 1.8 monolayers. The data are given in a linear and a logarithmic (Arrhenius plot) scale in (a) and (b), respectively. The heating rate was 2.0 K/s.

seen for xenon adsorption on Ru(001).¹⁸ The near coincidence of this phase transition temperature on Pt(111) with the gas-solid to gas-liquid phase transition at 98 K seems to be accidental, as can be seen by comparison with Ru(001) where there is no such match. Earlier quasiequilibrium measurements which show a drop of 30 meV in the isosteric heat upon the commensurate phase to compressed, striped incommensurate solid phase transition support this view.²² With further increasing xenon coverage (larger than 0.41) desorption from the second xenon layer can be seen, again with a common leading edge, for temperatures between 50 and 68 K [Figs. 2(a) and 2(b)]. In between the monolayer and second layer desorption in the temperature range between 68 and 88 K a constant nonzero xenon desorption rate is found, which is most likely due to thermal expansion of the dense xenon adlayer. Besides these features related to a well-ordered Pt(111) surface, there is a small xenon desorption peak at about 140 K which amounts to a coverage of about

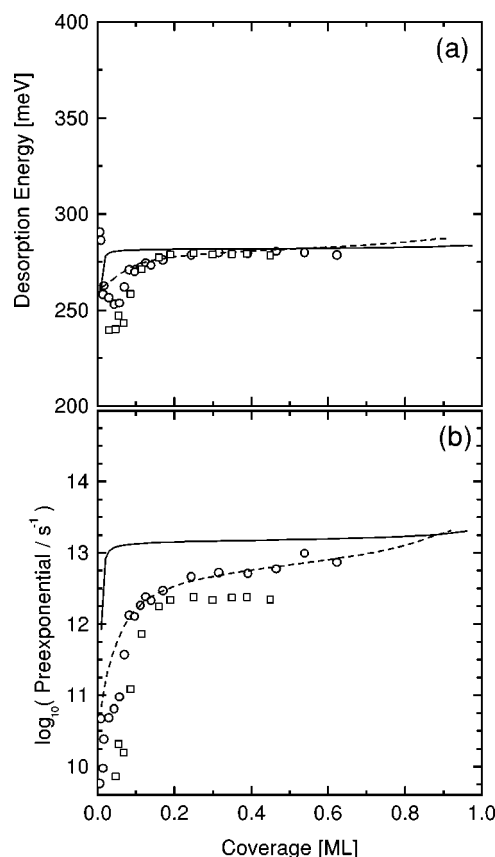


FIG. 3. Coverage dependence of the desorption energy and effective preexponential in the desorption rate for Xe/Pt(111). Open symbols: from leading edge analysis of the experimental data in Fig. 2(b) [circles and squares denote data for two different Pt(111) crystals with different defect concentrations]; solid line: from leading edge analysis of lattice-gas model spectra in Fig. 7; dashed line: from lattice-gas model fitting the experimental binding energy data with a reduced lateral attraction of -7 meV.

0.002 as is visible on the logarithmic scale in Fig. 2(b). We attribute this peak to xenon adsorption at defects, most likely steps due to a slight miscut of the crystal. Preadsorption of small amounts of CO or H₂ suppresses this peak (not shown here). The coverage of this peak can be used to estimate a lower limit for the average terrace width of 500 \AA .

A quantitative analysis of the leading edge for the data shown in the Arrhenius plot of Fig. 2(b), and further data not shown, yields the coverage-dependent desorption energies and preexponential factors, shown in Figs. 3(a) and 3(b), respectively. The data are marked by open circles and squares for two different (111) single crystals with defect concentrations of 0.018 and 0.006, respectively. For the second layer, not shown in Fig. 3, a desorption energy of 172 meV with a preexponential factor of about 10^{13} s^{-1} is found. The first layer possesses a desorption energy in the range 270–280 meV constant over the coverage range of 0.04–0.27 [0.10–0.65 of the saturated monolayer (ML)] with a preexponential between 2 and $8 \times 10^{12} \text{ s}^{-1}$, depending on the crystal. Some of this variation is also due to the details of the analysis, i.e., which part of the leading edge is used. Below a coverage of 0.04, but still well above the measured defect density of this crystal, reduction of the desorption energy to 250 meV and of the prefactor to $5 \times 10^{10} \text{ s}^{-1}$ are observed as

one would expect below the coexistence line where desorption occurs from a 2D gas phase where lateral (attractive) interactions are less effective. This reduction in desorption energy corresponds to a total lateral interaction of about 30 meV which is absent at sufficiently low coverages. At the lowest coverages around 0.008, the significant increase to 293 meV in desorption energy is attributed to xenon adsorption at defects, most likely steps. The further decrease of the prefactor to $5 \times 10^9 \text{ s}^{-1}$ is a consequence that zero-order desorption is assumed in the leading slope analysis (to get a constant prefactor over much of the desorption range) whereas below the coexistence region desorption will be closer to first order, i.e., a prefactor assuming zero order drops like θ . From our analysis of the TPD data, we conclude that coexistence breaks down at about 0.1 ML, which is slightly higher than the value of 0.07 ML (at a temperature of 100 K) extracted from the phase diagram of Poelsema *et al.*³ However, one should keep in mind that the Arrhenius analysis yields temperature-averaged quantities and a definitive phase boundary cannot be extracted.

To check the consistency of the leading edge Arrhenius analysis²³ of the TPD data we have recalculated the spectra with the desorption energies and prefactors of Fig. 3. For the second layer the overall features—peak positions and widths—are reproduced well. However, for the first layer there are two discrepancies with the original data, Fig. 2(a), namely, in the recalculated spectra the departure from the leading edge (just short of the maximum desorption rate) is more abrupt, i.e., in the region of the maximum the peak is not as rounded as in the experimental data; and the trailing edge drops to zero much faster, i.e., at lower temperature. To put it another way, the recalculated first layer TPD spectrum has more in common with the features of the second layer peak in Fig. 2(a), than with the first layer peak which it is supposed to reproduce. Although these discrepancies appear small and can only be seen because of the high quality of the data, they point to an interesting nonequilibrium effect.

We recall that the common leading edge of the dominant monolayer desorption is evidence for zero-order desorption from a two-phase adsorbate in internal equilibrium. By the latter we imply that in the temperature range of desorption, surface diffusion and adatom sublimation from the border of the condensed xenon islands are so fast that the adsorbate maintains the equilibrium structure at its actual temperature and the (remaining) coverage. Under such conditions the rate of desorption is proportional to the fugacity, $\exp(\mu/k_B T)$, where $\mu = \mu(\theta, T)$ is the chemical potential of the adsorbate. In the coexistence region the chemical potential is constant, and thus desorption is zero order. The main peak of the first layer desorption of xenon from Pt(111) is in the temperature regime 95–110 K, i.e., mostly above the 2D triple point at 98 K and well below the critical point at 120 K.³ In the temperature range of desorption the 2D gas phase is restricted to less than 0.07 ML (Refs. 3 and 11) and the chemical potential is constant above that up to a coverage near 1/3. Thus desorption will follow the leading edge until all but 0.07 ML are desorbed. As a result the break from the leading edge is abrupt and the desorption rate should drop to zero rapidly. The experimental data show neither the abrupt break nor the sharp dropoff. In the theoretical section, Sec. V, we will

show that this discrepancy is likely to be related to the lack of maintaining equilibrium in the adsorbate during desorption.

The nonequilibrium condition during desorption can be seen by an isosteric analysis²³ which, in principle, should produce the same desorption energies and prefactors as the leading edge analysis of the TPD traces shown in Fig. 3, provided that the adsorbate remains in quasiequilibrium during desorption. Plotting the rates for constant coverage against inverse temperature we do not get straight lines as required for an Arrhenius analysis. If we ignore this and do a least squares fit of straight lines to these isosteres anyway, we obtain desorption energies that drop linearly by 30% at low coverage, and prefactors that drop similarly by three orders of magnitude. However, the actual values for desorption energies and prefactors now depend on the temperature range over which the Arrhenius plots are evaluated (due to their curvature). This comparison of isosteric and leading edge analysis for the same high-resolution data shows clearly the consequent difference based on the fact that the analyzed desorption rates differ by orders of magnitude: During the low desorption rates analyzed within the leading edge, 10^{-5} to 10^{-3} ML/s, which corresponds to desorption of the 0.01-ML 2D gas phase in 10 to 1000 s, the equilibrium can be maintained. However, at the higher desorption rates relevant for the isosteric analysis—around 0.1 to 0.2 ML/s which defines a time scale of about 0.1 s for desorption of the 2D gas phase at a surface temperature of 105 K—the equilibrium breaks down. Although a recalculation of the TPD spectra with desorption energies and prefactors from the isosteric analysis, as we show in Sec. V later, gives a very good fit to the experimental data, the analysis itself is flawed (no straight isosteres) and the energies and prefactors by it bear no physical meaning. This is in contrast to the leading edge analysis for which the Arrhenius analysis gave equilibrium energies and prefactors which must be and actually are consistent with similar data extracted from equilibrium data. Obviously, nonequilibrium effects build up the most in the tails of the TPD spectra so that an isosteric analysis gives wrong desorption energies and prefactors particularly for low coverages/high temperatures.

B. Xe/Pt(997)

Thermal desorption spectra for xenon adsorption on Pt(997) are displayed in Figs. 4(a) and 4(b) on linear and logarithmic ($1/T$) scales, respectively. The main features seem to be quite similar to desorption from Pt(111), see Figs. 2(a) and 2(b): Monolayer desorption occurs around 102 K, the second layer—well separated from third and higher layers as on Pt(111) (not shown in Fig. 2)—desorbs between 62 and 67 K with a common leading edge, and there is again a region of constant but nonzero desorption in between the second and first layer desorption. However, there are three important differences to Pt(111). First, the desorption peak temperature of the dominant submonolayer desorption around 102 K is nearly constant with coverage and not upshifting as on Pt(111), and there is no common leading edge as can be seen best in Fig. 4(b). Clearly, xenon does not obey zero-order desorption kinetics on this surface. However, the absence of a peak shift does not imply the absence of lateral

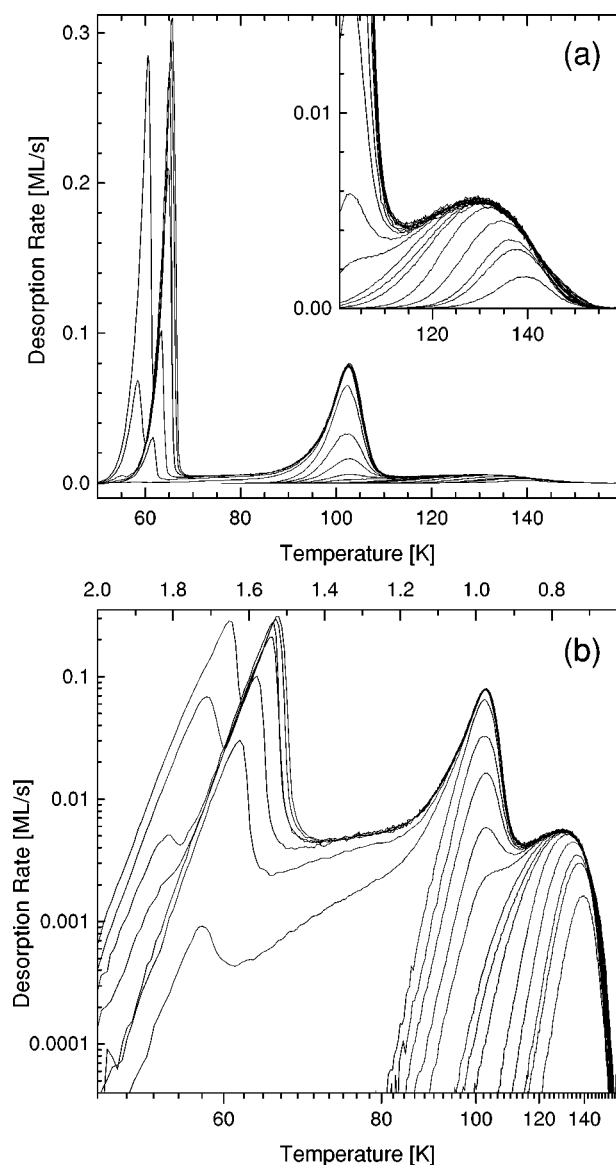


FIG. 4. Experimental TPD spectra for different xenon coverages on Pt(997) in the coverage range up to 2.8 ML. The data are given on linear and logarithmic (Arrhenius plot) scale in (a) and (b), respectively. The heating rate was 1.0 K/s.

interactions, as we will discuss later. Secondly, there is no phase transition feature on Pt(997) as had been seen around 94 K on Pt(111) for coverages above 0.33. Thirdly, there is a well-defined desorption feature in the temperature range of 110–150 K due to xenon adsorption at the step edges. This part of the desorption spectrum is amplified in the inset of Fig. 4(a). This “step peak” shifts with increasing coverage from 140 to 130 K and has a common trailing edge. It saturates at a coverage of 0.06 (relative to the number of Pt surface atoms, or 0.16 of the saturated monolayer, see below) before the dominant monolayer (terrace) desorption starts to grow.

Whereas the observation of a high-temperature desorption peak due to adsorption at the steps is expected for a stepped surface and has been reported previously, the first two observations demonstrate that xenon desorption from the close-packed (111) terraces on the stepped Pt(997) is also considerably different from that on the flat Pt(111) surface. The

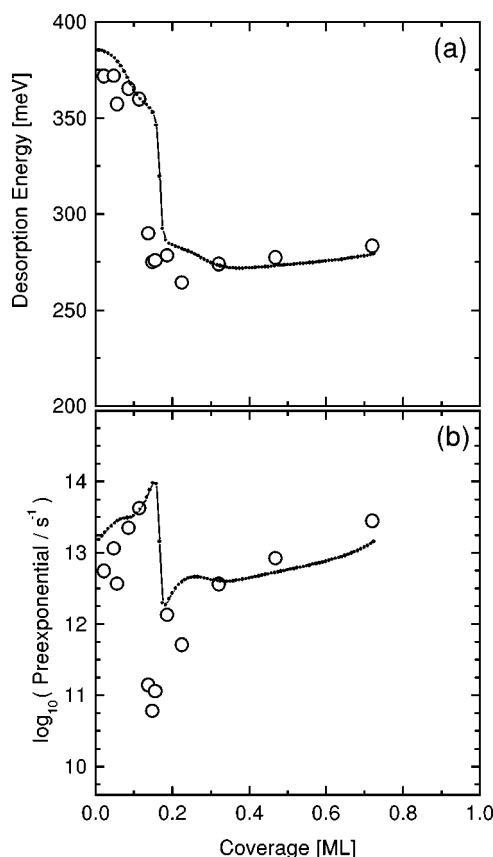


FIG. 5. Coverage dependence of (a) the desorption energy and (b) the effective preexponential in the desorption rate for Xe/Pt(997). Open circles: from leading edge analysis of experimental data in Fig. 2(b); lines: from leading edge analysis of model spectra in Fig. 9.

absence of zero-order desorption kinetics shows that there is no coexistence of 2D gas and condensate in the temperature range of the monolayer (terrace) desorption, i.e., the 2D critical temperature is considerably reduced compared to the flat Pt(111) surface. Since the critical temperature is also a measure of the lateral Xe-Xe interaction, one might expect a weakened lateral interaction on the terraces of the Pt(997). However, as we will discuss later together with the desorption simulations, there is actually *no* difference in the lateral interactions, and this issue is in fact closely related to the finite size of the (111) terraces.

In Figs. 5(a) and 5(b) the desorption energy and preexponential factor are shown as functions of xenon (submonolayer) coverage, as extracted from an Arrhenius analysis of the leading edge of the desorption traces.²³ For the second layer a desorption energy of 170 meV with a preexponential of about 10^{13} s^{-1} obtains (not shown in Fig. 5), as for xenon on Pt(111). For monolayer desorption the desorption energy of 280 meV and the preexponential of about 10^{13} s^{-1} are similar to the corresponding values on Pt(111) despite the fact that different desorption kinetics are observed. For coverages below 0.16 ML, i.e., for xenon adsorption at the step edges, a drastic increase in desorption energy up to 370 meV is observed, even higher than the defect-related value of the flat surface. The corresponding preexponential at lowest coverage of about $6 \times 10^{12} \text{ s}^{-1}$ has not changed profoundly. For completion of the xenon step decoration at 0.16 ML, there is

a reduction of the preexponential by two orders of magnitude. The presented data will be discussed together with the theoretical modeling (solid lines) below. To check for possible nonequilibrium effects we have also done an isosteric analysis which yields more or less the same desorption energies and prefactors as those from the leading edge analysis. Consequently, the recalculation of the TPD spectra with the extracted desorption energies and prefactors shows good agreement with the original data, in contrast to desorption from Pt(111). We conclude that, contrary to Pt(111), 2D equilibrium is maintained on this surface all the way up to desorption of the lowest coverages.

Note that we refrained from estimating error bars for the extracted values here for good reasons. While there is no question that an estimate of probable confidence limits of parameters extracted from experimental data is very important in general, there are specific problems here which are connected with the parametrization of kinetic data into desorption energies and preexponentials. For such cases as rates of thermal desorption it is well known that both quantities are coupled (compensation effect, window effect). This is particularly serious for data which do not span several orders of magnitude for the desorption rates, but even for our wider range of measurement one can get reasonable fits for different sets of parameters as long as the corresponding desorption rates are similar within the window of measurement. Therefore for an adequate treatment of errors some kind of "combined error" would have to be given which would be difficult to interpret. An alternative would be to define new quantities (linear combinations) which are independent from each other and could then be presented with their respective error bars. The latter approach—although mathematically straightforward—would also mask the underlying physical concepts. Because of these difficulties we have not given error bars for the desorption parameters explicitly. However, since we do not present a single extracted value (i.e., one desorption energy/prefactor pair) but sequences of coverage-dependent data points each of which is based on the independent evaluation of a spectrum, the statistical error bars may be well estimated from the statistical deviation within the data (Figs. 3 and 5). Even in these extracted values the mentioned compensation effect can be seen (look, for instance, at the third and tenth data points in Fig. 5). To further demonstrate the reproducibility and to give at least some idea of possible systematic errors, data from two *different* crystals have been presented (Fig. 3).

To demonstrate an additional, step-induced, difference between the Pt(111) and Pt(997) surfaces, we present in Fig. 6 the LEED structure measured at 25 K for xenon monolayer saturation on Pt(997). Close to the rim of the pattern the hexagonally positioned first-order spots of the (111) terraces with the characteristic splitting in the $[1\bar{1}0]$ direction due to the interference of the terraces separated by the steps can be clearly seen. Upon xenon adsorption an additional hexagonal structure appears with a lattice constant about 0.63 times that of the (111) substrate terraces. This pattern corresponds to an incommensurate, hexagonally close-packed xenon layer with a Xe-Xe distance of 4.4 Å which translates into a xenon saturation coverage of 0.40. It is a slightly wider structure than on Pt(111) which might be explained by stress relief at the step edges. The orientation of the hexagonal xenon struc-

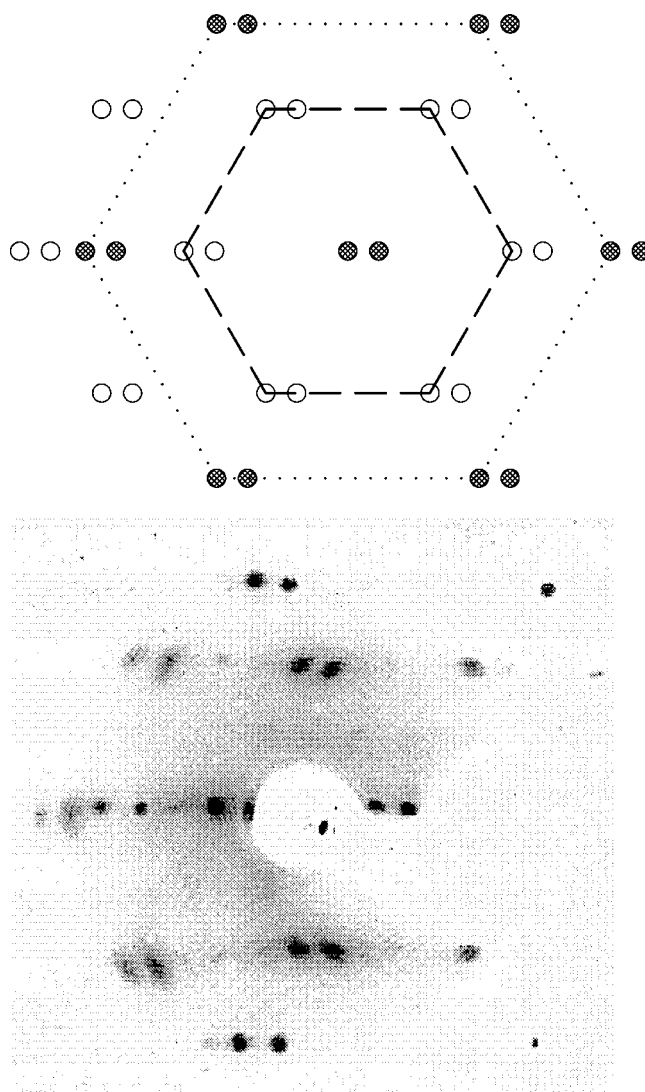


FIG. 6. LEED pattern for xenon adsorption on Pt(997) at saturation coverage. The pattern was recorded at an electron energy of 78 eV and at a temperature of 25 K. For clarity, the observed structure is sketched on the right: The overlayer spots are marked by open circles.

ture is aligned with the underlying Pt(111) structure as seen in Fig. 6, at variance with the observation on a flat Pt(111) where the structure is rotated by about 30° .⁶ Such step- (defect) induced reorientations (30° rotations) have been reported for krypton and argon on nominally flat Pt(111) surfaces.^{22,24} However, no such reorientation has been found for xenon on Pt(111).²⁵ Note the elongated, sickle-shaped form of the xenon spots in Fig. 6 which indicates xenon domains of different small angle rotation ($<3^\circ$) with respect to the substrate. This again underlines that the xenon saturation structure is incommensurate (or higher-order commensurate) with the substrate, i.e., does not lock into the substrate structure at *any* coverage. Additionally to this saturated nonrotated hexagonal close-packed structure we see at intermediate coverages also weak diffraction spots originating from some 30° rotated islands as on the flat Pt(111) surface. However, the dominant structure is the nonrotated one. For

xenon step decoration LEED shows weak streaks at half-order position, equivalent to a Xe-Xe distance of 5.56 Å, twice the Pt-Pt distance along the close-packed steps.

IV. THEORY

To model the adsorption and desorption of xenon on Pt(111) and Pt(997) one can safely assume that the geometrical structure of the metal surfaces is not affected by the adsorption of xenon. The surface thus provides a weakly corrugated potential with diffusion barriers that are small in comparison to the lattice structure imposed by the lateral interactions between adsorbed xenon atoms. However, the substrate corrugation is not altogether negligible because at least on Pt(111) there is a commensurate $(\sqrt{3} \times \sqrt{3})R30^\circ$ structure at coverage 1/3.

To model the various phases and structures of xenon on both surfaces would require a detailed and very precise knowledge of the Xe-Pt and Xe-Xe (many-body) interactions both at distances larger than the (average) xenon adlayer lattice constant (to model the ordered structures and domain walls accurately) and at shorter distances to understand the compressional phase. Despite great progress in the understanding of these interactions the level of accuracy is not sufficient for this task and we have to resort to simpler models rather than develop an all encompassing theory.

We will restrict our theoretical efforts to the coverage range below 1/3, i.e., before compressional effects come into play. Our primary aim is to understand the differences in the TPD spectra induced by the presence of the steps on Pt(997) and we will do this in the context of a lattice-gas model. A lattice-gas model is well defined for systems in which the surface of the solid provides localized adsorption sites which do not change in their geometric pattern as the coverage of the adsorbate increases, although the energetics of course can. As we argued earlier this is not the case for the present systems in which the lattice is defined by the lateral interactions in the adsorbate. Starting with the Pt(111) surface we will thus base the lattice-gas model on the lattice implied by the formation of xenon islands with $(\sqrt{3} \times \sqrt{3})R30^\circ$ structure on Pt(111) up to a coverage 1/3 and to temperatures above 60 K relevant for monolayer desorption. With this model we will be able to explain the TPD data for xenon on Pt(111) (up to initial coverages of 1/3 ML), including the subtle non-equilibrium effects. The reason such an oversimplified model can do this lies in the fact that desorption occurs mainly in the coexistence region. For the latter the chemical potential is constant as a function of coverage and its variation over the very narrow temperature range of desorption is rather small so that a model that can realistically describe coexistence should suffice, as will be shown. It is still worthwhile to indicate what this model fails to do. (i) Because the model imposes a rigid lattice structure it does not account for the additional entropy arising from nonlocalization, particularly at the lowest coverages. (ii) The domain wall structure will be different in a nonlocalized adsorbate from that in a lattice gas although one can argue that this should not be too important on Pt(111) where the structure in the adsorbate is imposed by attractive interactions. (iii) Changes in the lattice constant due to temperature or coverage variations are not possible in the lattice gas; however, they should have little

effect on the energetics of the system which is our primary concern. (iv) To repeat: any compression or change in orientation is not accounted for in the lattice gas. With these provisions we proceed to define a lattice gas for xenon adsorption keeping in mind that its applicability is restricted to coverages less than the maximum in the $(\sqrt{3} \times \sqrt{3})R30^\circ$ structure, i.e., in the present model the maximum coverage in a monolayer of xenon is 0.33 relative to the Pt surface atoms.

For xenon adsorption on an ideal Pt(111) surface we define a lattice gas as a hexagonal array of cells each containing one adsorption site which we label with an index i . Introducing occupation numbers $n_i^{(t)}$ [we have added a superscript t denoting terrace because we will shortly extend this model to Pt(997) and include two additional kinds of step sites] equal to zero or one depending on whether the i th adsorption site is empty or occupied. We can write the Hamiltonian of the system as²⁶

$$H = \sum_i E_t n_i^{(t)} + V_1^{(t-t)} \sum_{i,a} n_i^{(t)} n_{i+a}^{(t)}. \quad (1)$$

The first term in Eq. (1) accounts for the energy gain due to the interaction with the surface. This single-particle energy is given (for atoms) by

$$E_t = -V_t - k_B T \ln(q_3^{(t)}), \quad (2)$$

where V_t is the depth of the adsorption potential of a (terrace) site, and $q_3^{(t)}$ is the single-particle partition function of a particle adsorbed in this site accounting for its vibrations perpendicular and parallel to the Pt surface. The second term in Eq. (1) accounts for the lateral interaction between two particles adsorbed on nearest-neighbor cells. For xenon on Pt(111) this interaction is attractive to account for the formation of condensed islands. Further lateral interactions [which can be included straightforwardly in Eq. (1)] are necessary in particular to explain the details of the phase diagram such as the appearance of a solid-liquid phase transition at 98 K. To keep the model as simple as possible and to keep the number of parameters minimal, we will restrict it to nearest neighbor [and some next-nearest-neighbor on Pt(997)] interactions.

Turning next to the Pt(997) surface, we know from experiment that close to saturation at coverage 1/3 there are five rows of adsorbed xenon atoms (parallel to the steps) per terrace with a hexagonal structure. We will use this to define a lattice-gas model keeping in mind that our earlier comments on the shortcomings of a lattice-gas model for xenon adsorption on Pt(111) apply here as well (and perhaps even more so considering the more complicated LEED patterns). We will assume that there are three rows of adsorption sites on the terraces (t), as depicted in Fig. 1, with the e and b sites on the edge (e) and at the base (b) of the steps energetically different from the t sites in the interior of the terraces. Introducing additional occupation numbers, $n_i^{(e)}$ and $n_i^{(b)}$ equal to 0 or 1 depending on whether these sites are empty or occupied, we add the following terms to the Hamiltonian (1) of the system:

$$\begin{aligned}
& \sum_i (E_e n_i^{(e)} + E_b n_i^{(b)}) + V^{(b-b)} \sum_{i,a} n_i^{(b)} n_{i+a}^{(b)} \\
& + V^{(e-e)} \sum_{i,a} n_i^{(e)} n_{i+a}^{(e)} + V^{(t-e)} \sum_{i,a} n_i^{(t)} n_{i+a}^{(e)} \\
& + V^{(t-b)} \sum_{i,a} n_i^{(t)} n_{i+a}^{(b)} + V^{(e-b)} \sum_{i,a} n_i^{(e)} n_{i+a}^{(b)}. \quad (3)
\end{aligned}$$

All interactions between xenon atoms on adjacent sites are nearest neighbor, except for $V^{(e-b)}$ which crosses a step edge.

In our model of the adsorption-desorption kinetics we must account for the fact that for xenon on Pt(111) mass exchange or diffusion along the surface is apparently not fast enough (on the time scale of adsorption and desorption) to maintain the adsorbate in quasi-equilibrium at low residual coverages. Because xenon desorbs from Pt(111) out of the coexistence region of the dilute and condensed phases we assume that nonequilibrium builds up during desorption due to the limited exchange of particles between these phases but that the two phases are internally in equilibrium.²⁷ In such a situation the adsorbate can be characterized by the partial coverages θ_d and θ_c of the dilute and condensed phases, respectively. On the basis of nonequilibrium thermodynamics one can show²⁷ that they are subject to rate equations

$$\frac{d\theta_d}{dt} = R_{\text{ad}}^{(d)} - R_{\text{des}}^{(d)} + R_{\text{ex}}, \quad (4)$$

$$\frac{d\theta_c}{dt} = R_{\text{ad}}^{(c)} - R_{\text{des}}^{(c)} - R_{\text{ex}}, \quad (5)$$

where the rates of adsorption and desorption into the dilute phase are given by

$$R_{\text{ad}}^{(d)} = S(\theta, T) a_s \frac{\lambda}{h} P, \quad (6)$$

$$R_{\text{des}}^{(d)} = S(\theta, T) a_s \frac{k_B T}{h \lambda^2 q_3^{(t)}} e^{-V_i/k_B T} \frac{\theta_d}{1-\theta} e^{\mu_i^{(d)}(\theta_d, \theta, T)/k_B T} \quad (7)$$

and similar expressions for the condensed phase. Here a_s is the area of an adsorption site, P the instantaneous pressure, and $S(\theta, T)$ is the sticking coefficient.

Mass exchange between the condensed and dilute phases is controlled by the diffusion term which we could derive rigorously from a kinetic lattice gas.²⁸ However, because we know experimentally that nonequilibrium effects are secondary for xenon on Pt(111) [and even smaller on Pt(997)] we invoke nonequilibrium thermodynamics to get an approximate expression for the diffusion rate, namely,²⁷

$$R_{\text{ex}} = r_{\text{ex}} \left(e^{\mu_i^{(d)}(\theta_d, \theta, T)/k_B T} \frac{\theta_d}{\theta_d^{(0)}} - e^{\mu_i^{(c)}(\theta_c, \theta, T)/k_B T} \frac{\theta_c}{\theta_c^{(0)}} \right). \quad (8)$$

Here $\theta_d^{(0)}$ and $\theta_c^{(0)}$ are the equilibrium rates at the given total coverage and temperature. The rate r_{ex} we assume to be constant because we do not expect thermal activation to vary much over the temperature range of desorption.

The dependence of the desorption rate on the binding differences, including site frequencies, and the lateral interaction energies between t , e , and b sites is accounted for in the interaction part of the chemical potentials, $\mu_i^{(d)}(\theta_d, \theta, T)$ and $\mu_i^{(c)}(\theta_c, \theta, T)$. If the adsorbate is completely equilibrated then there is a unique chemical potential which we can calculate from the Hamiltonian (1). Moreover, in equilibrium we can determine the partial coverages from the phase diagram, i.e., for coverages less than the lower coexistence line we have $\theta_d^{(0)} = \theta$ and $\theta_c^{(0)} = 0$, for coverages larger than the upper coexistence line we have $\theta_d^{(0)} = 0$ and $\theta_c^{(0)} = \theta$, and within the coexistence region partial coverages are given by the Maxwell lever rule. Thus in equilibrium we can define the chemical potentials $\mu_i^{(d)}(\theta_d, \theta, T)$ and $\mu_i^{(c)}(\theta_c, \theta, T)$ uniquely, and it is these chemical potentials that we take in the desorption and mass exchange rates. A similar procedure was followed in an earlier study of nonequilibrium effects.²⁷

To calculate the coverage and temperature dependencies of the chemical potential we employ the transfer matrix method.²⁹ For the fcc(111) surface the transfer matrix is constructed for interactions between two adjacent parallel rows of M nearest-neighbor sites, with the occupation states of these sites indexing the matrix. $M=6$ gives good accuracy. For the fcc(997) surface a ‘‘row’’ consists of the five nearest-neighbor sites on the terrace. With the constraint of periodicity in this direction (i.e., the b site at the end of the row couples to the e site on the terrace above), two adjacent rows incorporate the interactions in Eq. (3). Unlike that for the (homogeneous) fcc(111) surface, the transfer matrix can no longer be block diagonalized. As discussed elsewhere,²⁹ the leading eigenvalue of the transfer matrix corresponds to the grand partition function and its corresponding eigenvector determines the probabilities of the allowed states of the adsorbate. In particular, the partial coverages, for the layers of xenon on Pt(111) or for the t , e , and b sites on Pt(997), are available as a function of coverage.

To complete the theory we need to specify the coverage dependence of the sticking coefficient appearing in Eqs. (6) and (7). It is a measure for the efficiency of energy transfer in adsorption and desorption. As such it cannot be obtained from thermodynamic arguments but must be calculated from a microscopic theory or taken from experiment. The latter gives a constant sticking coefficient of order 1 measured at low surface temperatures.¹⁹ However, no significant temperature dependence up to the desorption temperatures is expected.

V. THEORETICAL RESULTS

We use the lattice-gas model defined by the Hamiltonian (1) to explain the kinetic properties of xenon on Pt(111) and on Pt(997). The calculations proceed as follows: Once the Hamiltonian is specified and a set of interaction parameters is chosen, we construct the transfer matrix as discussed above. From this calculation we determine the chemical potential $\mu_i(\theta, T)$ self-consistently as a function of coverage and temperature, which allows us to determine equilibrium properties (isobars, the heat of adsorption, and entropy changes), and the desorption rate from Eqs. (4) and (5).

A. TPD of xenon from Pt(111)

In our attempt to model the TPD spectra of Fig. 2, we ignore the small structure around 95 K because for modeling the domain wall phase we would need longer ranged forces than those included in the Hamiltonian (1), and the incommensurate phases cannot be handled by this lattice-gas model anyway.

At very low initial coverage one can ignore the lateral interactions between adsorbed atoms, and the adsorbate is completely controlled by the single-particle properties, i.e., the binding energy of a single atom to the surface and the vibrational frequencies with respect to the surface. Although the quality of the TPD data at low coverage is such as to clearly exhibit desorption from the defect sites, we are primarily interested in modeling the (111) sites, and thus ignore the defect sites in this fit as we will discuss desorption from steps extensively in the next section. Also, representing these defect sites (steps, kinks, etc.) accurately within a lattice-gas model is difficult. So, rather than fit a *complete* low-coverage TPD trace to get the single-particle parameters in Eq. (2), we use the fact that the leading edge of zero-order desorption is controlled (i) by the energy of a particle in the coexistence region, $E_t + 0.5cV^{(t-t)}$, where E_t is the single-particle energy in the first layer [see Eq. (2)], $V^{(t-t)}$ is the nearest-neighbor interaction, and $c(=6)$ is the coordination number of the lattice, and (ii) by the vibrational frequencies of a particle with respect to the surface. For a lattice-gas model on a hexagonal lattice, the nearest-neighbor interaction (between xenon atoms in the first layer) is related to the critical temperature (of the first layer), $T_{\text{crit}}=120$ K, by $V^{(t-t)} \approx -1.10k_B T_{\text{crit}} \approx -11$ meV.³⁰ As for the vibrations of xenon atoms with respect to the surface we take for the perpendicular component the experimental value $\nu_z^{(t)} = 0.9 \times 10^{12}$ s⁻¹.³² This leaves us with only two free parameters, i.e., V_t and $\nu_x^{(t)} = \nu_y^{(t)}$ to fit the main desorption peaks from the first layer. Normally one would fit the peak positions and the widths of the desorption traces, or for the Arrhenius plot of Fig. 2(b) the slope and the width. However, because this system does not remain in quasiequilibrium throughout desorption we cannot model the width in this figure and are therefore left with the task to fit the slope and the intercept of the leading edge with two parameters. The vibrational partition functions in Eq. (7) contribute to the (differential) desorption energy in the coexistence region,

$$\begin{aligned} E_d(\theta, T) &= k_B T^2 \partial(\ln R_{\text{des}}) / \partial T \Big|_{\theta} \\ &= V_t - 3V^{(t-t)} + 2.5k_B T + \sum_i \frac{1}{2} h \nu_i \\ &\quad \times \{1 - 2/[1 - \exp(-h \nu_i / k_B T)]\}. \end{aligned} \quad (9)$$

This reduces in the low- and high-temperature limits to $V_t - 3V^{(t-t)} + 2.5k_B T + \frac{1}{2} \sum_i h \nu_i$ and $V_t - 3V^{(t-t)} - \frac{1}{2} k_B T$, respectively. In the intermediate-temperature region, which applies here, the vibrational modes contribute to both the slope and the intersection of the rates. We have chosen the two free parameters to reproduce the experimental (constant) desorption energy and prefactor in the coverage range $0.1 < \theta < 0.9$ which gives as the well depth [Eq. (2)] $V_t = 253$ meV and $\nu_x^{(t)} = \nu_y^{(t)} = 0.3 \nu_z^{(t)}$, see Fig. 7(a) or 7(b). Note that the break

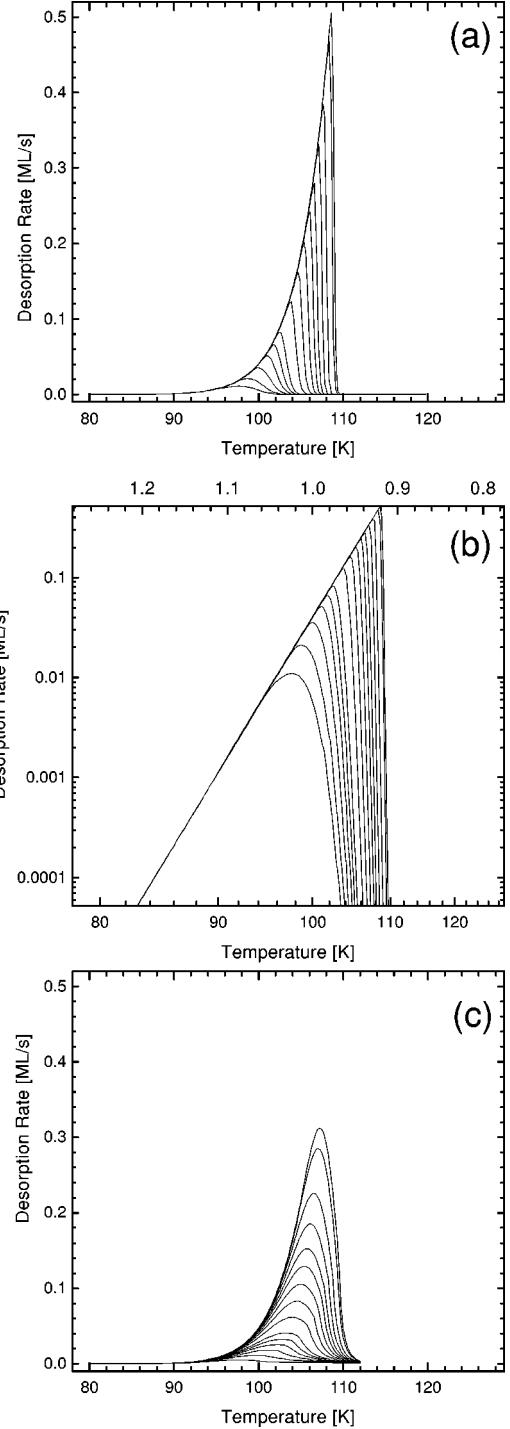


FIG. 7. Calculated TPD spectra for Xe/Pt(111). Lattice-gas parameters: $V_t = 253$ meV, $V^{(t-t)} = -11.2$ meV, $\nu_z^{(t)} = 0.9 \times 10^{12}$ s⁻¹, $\nu_x^{(t)} = \nu_y^{(t)} = 0.3 \times 10^{12}$ s⁻¹, $a_s = 16.7$ Å². (a) Linear plot with initial coverages of experiment up to one xenon monolayer (defined here as 0.33 relative to Pt), 0.031, 0.058, 0.086, 0.115, 0.142, 0.173, 0.247, 0.319, 0.393, 0.468, 0.539, 0.636, 0.751, 0.912, and 0.98; (b) logarithmic plot [(a) and (b) for quasiequilibrium model], and (c) nonequilibrium model.

from the common leading edge is very abrupt (contrary to the experimental data) because desorption occurs some 25 K below the critical temperature where only a few percent of a monolayer remains below the coexistence line. The discrepancies between Fig. 7(a) and Fig. 2(a) are partly due to non-

equilibrium conditions during desorption but exhibit also limitations of our simple approach: The lattice-gas model with restriction to nearest-neighbor interactions cannot describe the correct coverage (0.07 ML) (Ref. 3) at which the phase coexistence breaks down at a given temperature *and* at the same time reproduce the correct critical temperature (120 K). This can be seen from the theoretical desorption energies $E_d(\theta)$ and preexponentials in Figs. 3(a) and 3(b). At low coverages the breakdown of coexistence can be estimated from the deviation of constant desorption parameters to about 0.02 ML. On the other hand, trying to model both desorption parameters directly, as shown in Fig. 3 as a dashed line, leads to a reduced lateral interaction of about 7 meV. This leads within our model to a critical temperature of 89 K and therefore prevents coexistence with zero-order desorption, as is directly visible from the nonconstant desorption parameters at higher coverages. We have chosen to reproduce the correct critical temperature which also leads to about the same lateral attraction as the direct analysis of the experimental data.

We proceed to remedy the discrepancy in the break from the leading edge in the main submonolayer peaks which we discussed in the experimental section as being mainly due to nonequilibrium effects.³¹ Leaving all the energies and vibrational frequencies the same as in Figs. 7(a) and 7(b) we solve the rate equations for a finite diffusion rate constant ignoring again defects for simplicity. The resultant spectra, Fig. 7(c), obtained by fitting approximately the peak heights, clearly display the early break from the leading edge, the rounding of the peaks, and the consequent broadening. The diffusion rate is found to be comparable to the desorption rate at the peaks. The inclusion of defects moves the low initial coverage peaks to higher temperature.

The results of leading edge and isosteric Arrhenius analyses of the theoretical spectra using the ASTEK software package are displayed in Fig. 3. As indicated, this is all in good agreement with the analysis of the experimental data, as we should expect, having fitted the main features of Fig. 2 accurately. For the interpretation of the effective prefactor we note that its value and its interpretation depends on the choice of the desorption order. We emphasize that desorption is a process of well-defined order only in the absence of lateral interactions, e.g., at sufficiently low coverages. Otherwise its choice is arbitrary and should be made wisely. If we choose zero then $\nu_{\text{eff}}(\theta)$ will drop to zero at zero coverage and it is not the effective attempt frequency of a desorbing particle. For xenon desorption, on the other hand, one would argue that at vanishingly small coverages lateral interactions become unimportant and desorption should be first order. However, xenon desorption over most of the coverage regime is zero order and we should assume this. The prefactors for this choice for the experimental and the theoretical spectra are both plotted in Fig. 3.

Concluding, the modeling of the TPD spectra determined the desorption energy of the dominant monolayer desorption to a single-particle binding energy of 253 meV with an attractive pairwise next-neighbor interaction of 11 meV, in agreement with the simpler evaluation of the experimental data. Within the coexistence of 2D gas and condensed phase with six next neighbors this leads to a total lateral interaction of about 33 meV and to an apparent desorption energy of

286 meV. These values agree with the leading edge analysis of the experimental data which gives 250 meV for the 2D gas phase and a constant value of 280 meV for the coexistence region. Because of the nonequilibrium conditions the isosteric analysis had to fail as has been discussed in detail above.

B. TPD of xenon from Pt(997)

To understand the changes in the TPD spectra as we go from the Pt(111) to the Pt(997) surface, we proceed in stages. First we discuss the necessity of additional model parameters to describe xenon desorption from the stepped surface and their influence on different parts of the TPD spectra. Subsequently, we present a realistic fit to the experimental data. Lastly we show qualitatively how finite-size effects due to a narrowing of the terrace width destroy coexistence in the adsorbate layer and thus preclude zero-order desorption.

To determine the model parameters for the TPD spectra of xenon desorbing from Pt(997), we start initially by fitting the positions of the step and terrace peaks while ignoring lateral interactions. Specifically we assign binding energies V_e for edge and V_t for terrace adsorption in Eq. (3) to fit the experimental rate curves. To keep the number of free parameters to a minimum we take initially the binding energy of xenon on the terraces and at the bottom of the steps to be the same, $V_t = V_b$, and equal to that on Pt(111). We also chose the vibrational frequencies to be those for Pt(111) for both step and terrace sites. The result is shown in Fig. 8(a). Three features are unacceptable on comparison with Fig. 4(a), namely (i) the widths of the two peaks, (ii) the downshift of the main peaks, and (iii) the valley between them. To narrow the terrace peaks and at the same time to compensate for their downshift we need a small attraction between xenon atoms adsorbed on the terraces. This is to be expected because xenon adsorption on the terraces should be similar to that on Pt(111) where there is a strong nearest-neighbor attraction of $V^{(t-t)} = -11$ meV. For the Pt(997) surface introduction of terrace nearest-neighbor attraction (-7 meV) is illustrated in Fig. 8(b). To broaden the high-temperature peaks and to fill in the valley we need a significant repulsion between xenon atoms adsorbed on the step edges. The effect on TPD is shown in Fig. 8(c), where we have retained the attraction on the terraces of Fig. 8(b). This then yields a reasonable fit to the experimental spectra.

As we have shown step by step in Figs. 8(a)–8(c), the modeling of high-resolution TPD data is able to determine the binding energies of three different sites as well as the lateral Xe-Xe interaction within the terrace and along the steps. However, further parameters affect the form of the TPD spectra less and are therefore not uniquely extractable from TPD data alone. Thus to fill in the valley at 110 K between the peaks which is still visible in Fig. 8(c) and is absent in the experimental data, we have to introduce an additional species, e.g., xenon at the bottom of the step edge (*b* site), which has a higher binding energy than on the *t* sites. This also results in preferential island growth from the bottom of the steps. Also we impose a small repulsion between the *t* and *e* sites because it is known that the growth on the terraces is outwards from the bottom of the steps.¹⁰ For the same reason we have an attraction between the *t* and

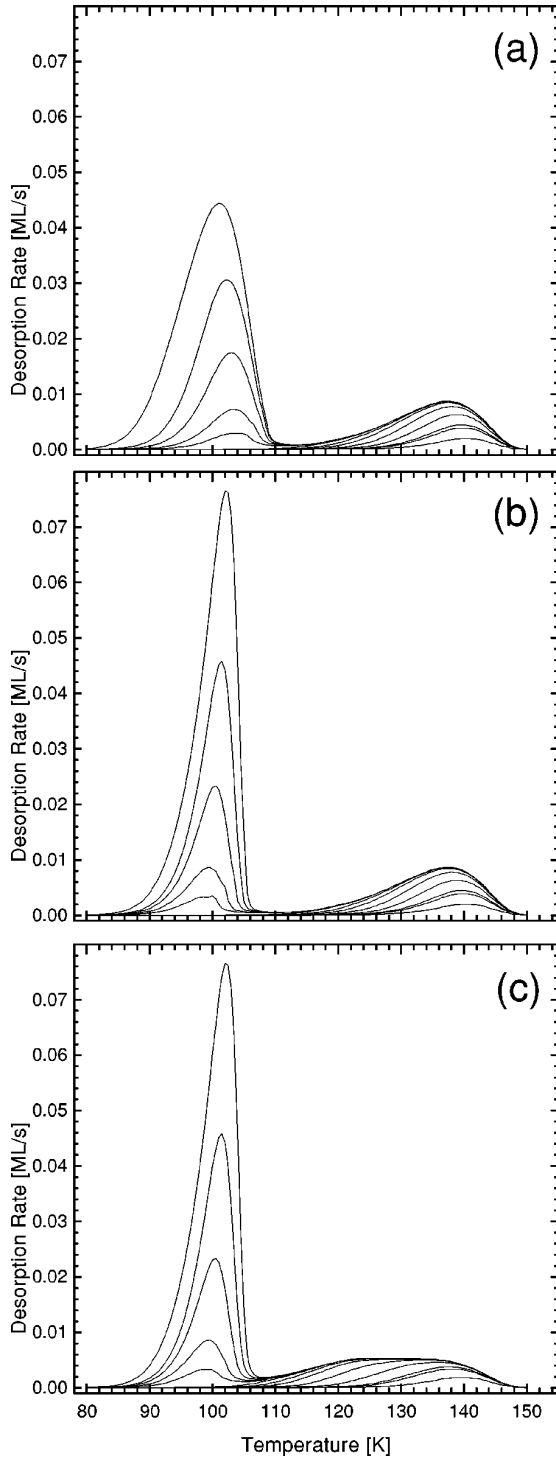


FIG. 8. Model TPD spectra for desorption from the first monolayer on a fcc(997) surface, with b sites bound identically to t sites, to show the influence of lateral interactions. Site binding parameters [frequencies as for Pt(111)]: (a) $V_t = V_b = 281$ meV, $V_e = 398$ meV; no lateral interactions. (b) As before, but $V_t = V_b = 267$ meV, terrace attraction $V^{(t-t)} = -6.9$ meV. (c) As (b), but additionally step repulsion $V^{(e-e)} = 15.9$ meV.

b sites (all on one terrace) slightly less than that of the t sites. The final result of this modeling is shown in Figs. 9(a) and 9(b). The binding energies are determined to be 264, 398, and 287 meV for xenon adsorption on the terrace, at the step edge, and at the bottom of the steps, respectively. The pair-

wise lateral interactions are -11.2 meV attractive on the terrace site and 15.9 meV repulsive along the step edge. To account for all data the additional lateral interactions between the species come out (less well defined) to be -4.3 meV attractive between the terrace and the bottom site, slightly (4.3 meV) repulsive between the edge and the terrace site, and negligible between the bottom and the edge site. The agreement with the experimental data is very good except in the valley where desorption from the edge sites and the b and t sites competes. There is also some residual desorption at the highest temperatures (probably due to additional more tightly bound defects such as kink sites along the steps) which we have not attempted to reproduce. The partial equilibrium coverages of the t , e , and b sites, as shown in Fig. 9(c) for three different temperatures, reveal a two-line growth in that first the e sites are completely occupied, and then the b sites fill in with the t sites trailing. This picture is confirmed by the partial desorption rates in Fig. 9(d) and also by the site-site correlators in Fig. 9(e). The results of an Arrhenius analysis of the theoretical spectra appear in Figs. 5(a) and 5(b) for comparison with the experimental data. The coverage dependence of the desorption energy and of the preexponential is well reproduced.

Concluding, the modeling of the TPD spectra revealed a desorption rate for xenon step decoration which should shift down from 398 meV at zero coverage to about 365 meV at completion of the step decoration due to the repulsive interaction. The extracted values from the leading edge analysis of the experimental data, up to 370 meV, are slightly lower. Furthermore, one has to keep in mind that any change of the Xe-Xe distance along the steps during desorption is beyond the possibilities of the lattice-gas model presented here.

For the clear illustration of the finite-size effect introduced on the stepped surface we will again simplify the model. We assume that adsorption on the terrace and at the bottom of the steps is identical. For their binding energies, vibrational frequencies, and lateral interactions we take the values obtained for the flat Pt(111) surface. Furthermore we ignore lateral interactions between e and b or t sites. For this illustration only the lateral interaction on the terrace (11 meV) is important, since the desorption parameters for the edge sites do not affect the onset of terrace desorption.

The effect of different terrace widths on desorption is shown in Fig. 10. Here we present calculated TPD spectra for two surfaces, one with seven xenon adsorption rows per terrace in Figs. 10(b) and 10(d), and one with five rows per terrace [i.e., more appropriate for xenon on Pt(997)] in Figs. 10(a) and 10(c) which can be compared to the flat (111) surface. For the seven-row surface (with five rows of t sites, one row of b sites and one row of e sites) near zero-order desorption, and thus coexistence in the desorption regime, is still very much in evidence as can be seen best at the common desorption onset in Fig. 10(d) and as it would be for wider terraces and obviously on the Pt(111) surface [Fig. 7(b)]. On the other hand, for the five-row surface (with three rows of t sites, one row of b sites, and one row of e sites) zero-order desorption visible as common leading edge, and thus coexistence in the desorption regime, is no longer possible for the same lateral interactions. Shifting the TPD spectra for the five-row surface down by 20 K by reducing the binding energies (but keeping the lateral interactions the

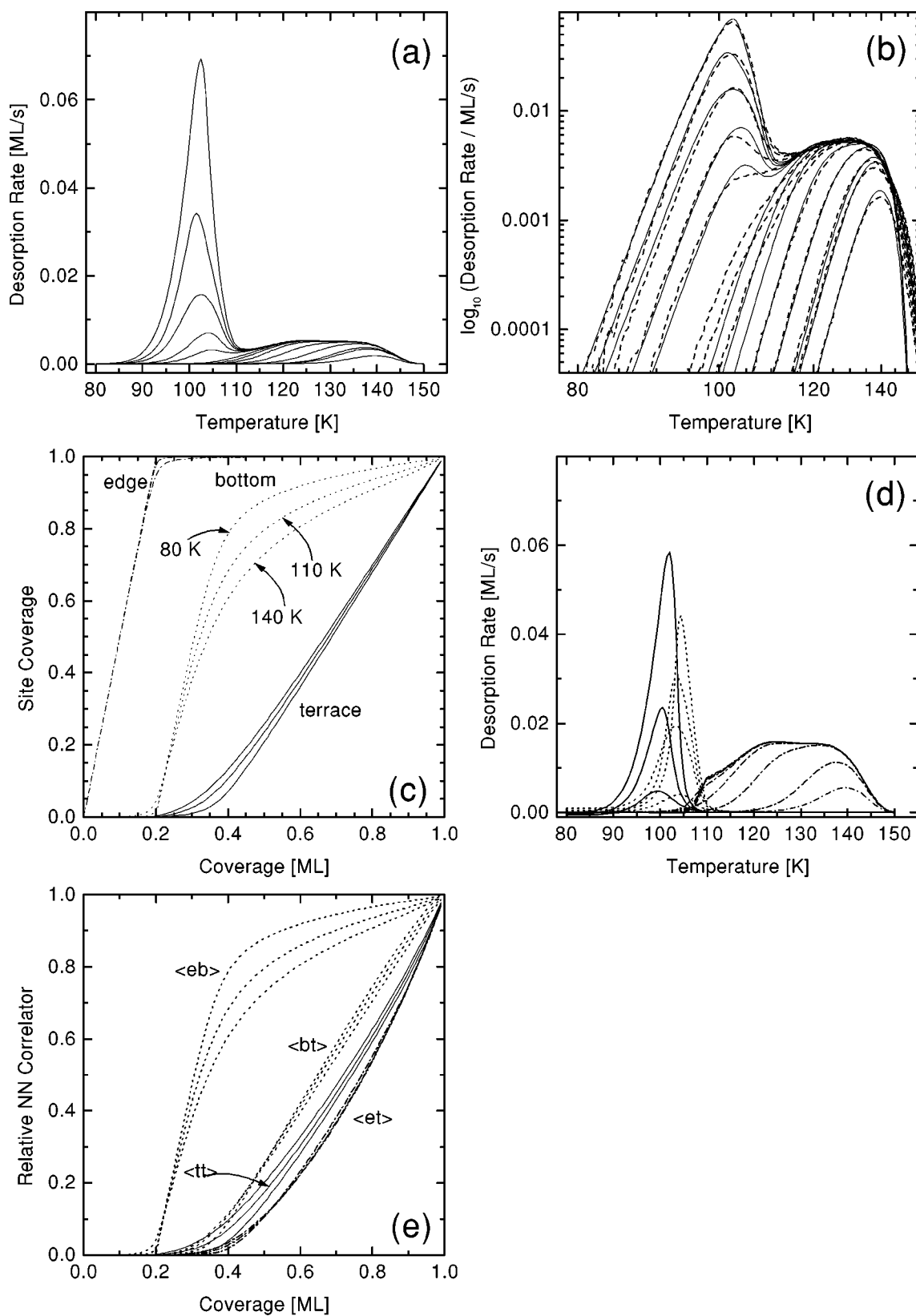


FIG. 9. Calculated TPD spectra for the first monolayer of xenon on Pt(997). Lattice gas parameters: $V_t=264$ meV, $V_b=287$ meV, $V_e=398$ meV. Interactions are $V^{(t-t)}=-11.2$ meV, $V^{(t-b)}=-4.3$ meV, $V^{(t-e)}=4.3$ meV, $V^{(e-e)}=15.9$ meV, $V^{(e-b)}=0$. (a) Linear and (b) logarithmic plots (dashed: experiment). (c) Partial coverages for 80 (sharpest features), 110, and 140 K: $5\theta_e$, $5\theta_b$, and $\frac{5}{3}\theta_t$, as indicated. (d) Partial rates (from left to right) $d\theta_t/dt$, $1.5(d\theta_b/dt)$, $3(d\theta_e/dt)$. Every other trace of (a) is omitted for clarity, except around the low-temperature peak. (e) Two-site correlators for the temperatures of (c).

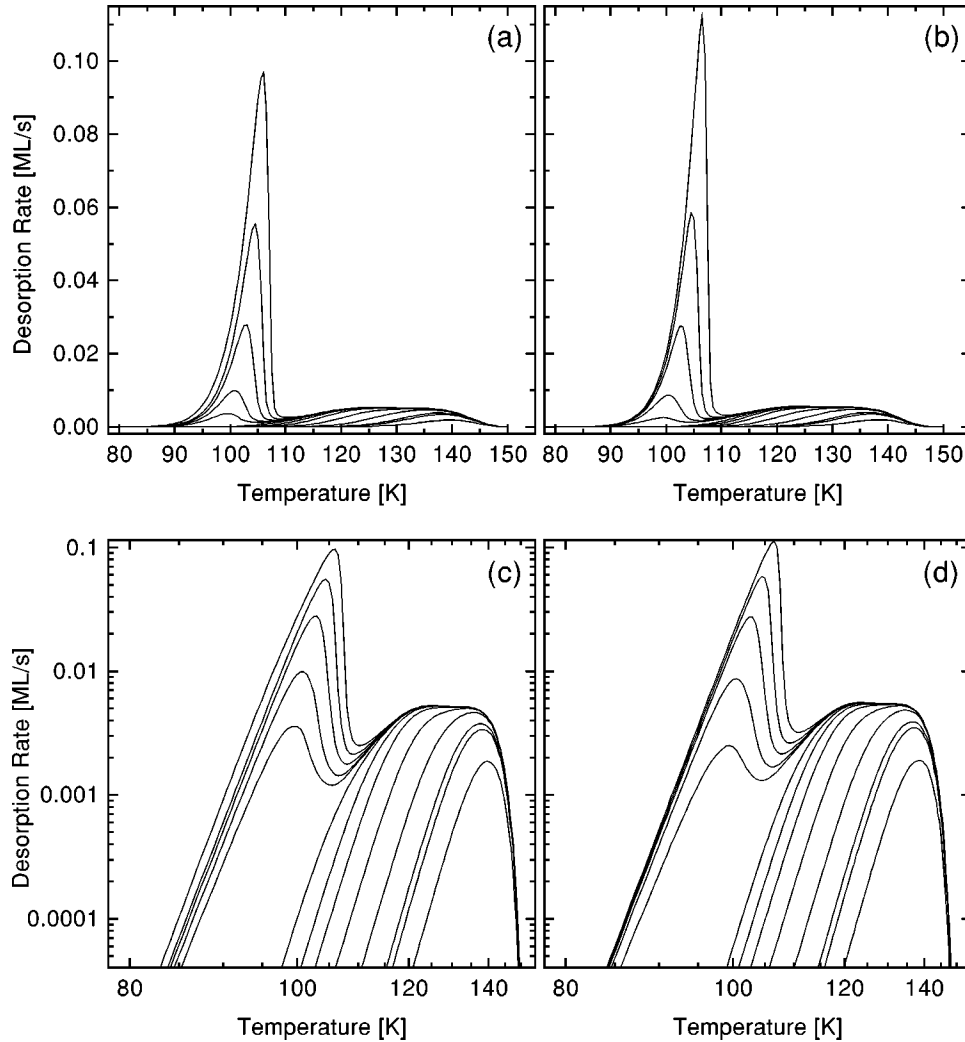


FIG. 10. Calculated xenon TPD spectra for desorption from stepped surfaces with different terrace widths. (a) Terrace with five xenon rows as for Pt(997); (b) wider terrace with seven xenon rows. Parameters as for Fig. 8(c), but lateral attraction $V^{(t-t)} = -11.2$ meV; (c), (d) corresponding logarithmic plots.

same) would result in a leading edge of the same quality as for the seven-row surface in Figs. 10(b) and 10(d). As is clear from this comparison, the finite size of the terrace width and the corresponding length restriction for xenon islands influence the thermodynamic properties significantly. The absence of lateral interactions between e and b or t sites decouples the terraces from each other and the adsorbate on each terrace becomes finite in the direction perpendicular to the steps.

As we have shown above, the complete modeling of the TPD spectra is consistent with a pairwise lateral attraction of 11 meV on the terraces as on Pt(111). However, if one starts modeling on a (wrong) seven-row surface the lateral interaction appears to be lowered to half the value within a reasonable fit. This emphasizes clearly the importance of the correct description of the adsorption geometry for meaningful modeling.

VI. DISCUSSION

For xenon desorption on the flat Pt(111) surface we deduce from the modeling a single-particle binding energy of 253 meV with an attractive pairwise next-neighbor interac-

tion of 11 meV taken from the critical temperature. Within the coexistence of 2D gas and condensed phase with six next neighbors this leads to a total lateral interaction of 33 meV and to an apparent desorption energy of 286 meV. These values agree with the leading edge analysis of the experimental data which gives 250 meV for the 2D gas phase and a constant value of 280 meV for the coexistence region. Our single-particle energy agrees well with the value of Rettner, Bethune, and Schweizer for this system¹² of 245 meV which was measured by molecular beam techniques over several orders of desorption rate magnitude (after masking defects by CO adsorption) in a coverage range of 1–5 % of the monolayer and therefore in the absence of significant lateral interactions. On the other hand, our constant desorption energy for the 2D gas-condensed phase equilibrium as well as the low-coverage value are considerably smaller than the results by Kern *et al.*^{22,33} from quasiequilibrium measurement of the isosteric heat: these authors report an increase from 277 to 312 meV over a wider coverage range than expected from the phase diagram.

Our extracted attractive pairwise lateral interaction (11 meV from the critical temperature in the TPD modeling and

10 meV from the desorption energy change of the experimental data) might be summed over the $c=6$ next neighbors, $0.5cV^{(t-r)}$, to 33 and 30 meV. This total lateral interaction within the condensed phase can be compared to the heat of evaporation for the 2D gas to condensed phase transition. The difference of 35 meV of the measured isosteric heats for a 2D gas with respect to the solid^{22,33} is close to our values. However, the value of 48 meV measured by Poelsema, Verheij, and Comsa³ is about 50% higher, which is close to the value discussed in the theoretical work of Gottlieb and Bruch.³⁴

The lateral interaction of xenon on transition metal surfaces has been discussed and simulated either on the basis of modified Lennard-Jones 6-12 potentials, e.g., Refs. 34–36 and references therein, or based on empirical potentials fitted to experimental data.³⁷ The dominant contributions are the gas-phase pair potential³⁸ which is close to the Lennard-Jones potentials around the potential minimum, the static dipole-dipole interaction which is often estimated based on the work function change upon xenon adsorption, and a substrate-mediated dispersion energy due to substrate response (image dipoles) on fluctuating adatom dipoles.³⁵ In the following we will estimate the different contributions based on a simple approach.

On Pt(111) Schönense³⁹ found a work function change of 0.6 eV upon xenon saturation which corresponds (via dividing by the number of xenon atoms per unit area) to a dipole moment of 0.53 D. Assuming localized dipoles within the xenon layer as is often done and summing up the dipole-dipole repulsion (ignoring any depolarization effects) within the hexagonal xenon lattice leads to an interaction energy of about 19 meV. In view of this repulsive interaction the experimentally determined resulting total attractive interaction of about 30 meV for the condensed phase points to a van der Waals interaction (substrate-mediated effects included) on the order of 50 meV. This value can be compared with the value based on the gas-phase potentials. Actually, the well-known gas-phase Xe-Xe pair potential³⁸ which can be approximated by a Lennard-Jones 6-12 potential ($\sigma=3.87$ Å, $E_B=25$ meV) around the minimum would predict an attraction around 80 meV, at a Xe-Xe distance of 4.4 Å. In the work of Gottlieb and Bruch to simulate the uniaxially incommensurate-to-commensurate phase transition for xenon adsorbed on Pt(111), the lateral Xe-Xe interaction was modeled by two different potentials: (i) similarly to the approach here by a pairwise Lennard-Jones potential ($\sigma=4.05$ Å, $E_B=20$ meV) leading to 67 meV attraction and (ii) by a multi-parameter potential constructed in analogy to earlier work on Xe/Ag(111) leading to an attraction of 51 meV at a Xe-Xe spacing of 4.4 Å.³⁴ Based on these comparisons it appears that we can get an estimate on the total Xe-Xe lateral interaction as sum of the attractive van der Waals (Lennard-Jones) potential and the repulsive dipole-dipole interaction based on work function changes.

Although this estimate seems to reproduce the correct order of magnitude for the lateral interaction, we emphasize that this is a rather oversimplified model. Modification of the metal *sp* surface state due to xenon adsorption which has been proposed to explain the significantly different lateral Xe-Xe interactions on platinum and palladium surfaces⁴⁰ has to be considered. Furthermore, we are well aware of high-

level local density calculations which go beyond a simple physisorption (van der Waals) picture for xenon adsorption.⁴¹

For xenon adsorption on the stepped Pt(997) surface we found preferred adsorption at the step edges with a single-particle binding energy of 398 meV and a repulsive pairwise repulsion of 15.9 meV along the xenon chains decorating the step edges. This strong repulsion leads to a Xe-Xe distance of 5.5 Å (twice the Pt-Pt distance) at 25 K as seen by LEED. With completion of step decoration, terrace adsorption starts with a second, slightly preferred adsorption site which might be assigned to adsorption at the bottom of the step edge. This would explain the xenon line-by-line growth on this surface as was seen by helium atom scattering for the first two xenon lines⁹ and is in agreement with STM studies.^{12,13} It might also explain the 30° rotation of the xenon hexagonal structure as compared to the (111) surface which has been seen by LEED.

For xenon step decoration on Pt(997) we measured a work function change of 0.47 eV compared to the bare surface. Accounting for the number density of xenon atoms, this converts to a dipole moment of 1.4 D, significantly higher than on the flat surface. Adding the interactions along the xenon chain results in a dipole-dipole repulsion of 17 meV at the observed next-neighbor distance of 5.54 Å. However, reducing this distance to the value of 4.4 Å as for the saturated layer would double the repulsion since the distance enters to the third power. Taking the Lennard-Jones potential by Gottlieb and Bruch as estimate for the lateral van der Waals potential and summing up this interaction within the chain leads to 21-meV attractive interaction at 4.4 Å. However, at the experimentally observed distance of 5.54 Å the attraction is reduced to 10 meV. The resulting lateral interaction from the sum of Lennard-Jones and dipole-dipole potential is therefore estimated to 7 meV repulsive which is a factor of 2 smaller than derived from the modeling. However, one has to remember that we ignored any lateral interaction due to a corrugation of the Xe-Pt potential which might be more important for adsorption at step edges.

Terrace saturation upon further xenon adsorption on Pt(997) reduces the work function further by 0.32 eV. Assuming in a simple picture that the step dipoles are not much affected, ignoring any depolarization next to the steps, and accounting for the reduced terrace size results in a dipole moment of 0.34 D, about 2/3 of the value on Pt(111). This might mislead to the conclusion of a reduced total dipole-dipole interaction; however, interaction with the strong dipoles at the step edges has to be included. Based on the reservations discussed above regarding this simple reasoning the close estimate to the experimental values seems accidental.

The binding energy (264 meV) is similar and the lateral interaction (11 meV) for xenon adsorption on the terraces of the stepped surface are the same as the values on the (111) surface. Nevertheless, the experimental spectra show different desorption orders—zero-order desorption on Pt(111) and first-order desorption on Pt(997)—in this coverage range. This pronounced difference in view of similar lateral interaction strengths on both surfaces is striking. It is explained by a breakdown of the 2D gas-condensed phase coexistence

which is responsible for the zero-order desorption on Pt(111).

As we have seen in the simplified model (lateral interaction only within the terrace), coexistence in the desorption range is destroyed once the terraces are narrow enough. This finite size smears out all thermodynamic singularities and discontinuities at the phase boundary and at the critical point, and lowers the critical temperature. The additional changes in the more realistic fit in Fig. 9 are due to the interactions across the steps which have been ignored for the discussion of the finite-size effect. This, on the one hand, makes the system large again in the direction perpendicular to the steps but, on the other, introduces considerable heterogeneity because most of these interactions are repulsive. This heterogeneity not surprisingly reduces the coexistence regime to well below the desorption range and, if strong enough, will prevent coexistence altogether. To see what is likely in the case for our system we have (artificially) reduced the binding energy of all sites by about one-third so that the main TPD peak occurs now around 60 K and actually displays a quasileading edge, similar in appearance to that in Fig. 10(a). This leads us to estimate that the critical temperature for xenon on Pt(997) (if it exists) should be less than 70 K.

To understand why xenon desorption from Pt(997) shows much less nonequilibrium effect than it does on Pt(111), we recall our argument that on Pt(111) nonequilibrium develops during desorption because the mass exchange between the dilute and the condensed phase is too slow on the time scale of desorption. This process is irrelevant on the Pt(997) surface in the temperature range of desorption because there is no coexistence there. In other words, it is the finite size of the system that enables the adsorbate to maintain itself in quasi-equilibrium during desorption from the Pt(997) surface.

VII. CONCLUSIONS

In this study we have presented xenon high-resolution thermal desorption data for the flat Pt(111) and the stepped Pt(997) surfaces supplemented by LEED data. By a leading edge as well as isosteric analysis to the data and by applying a detailed lattice-gas model to simulate the experimental data, we were able to quantify the lateral interactions within the layers as well as the strengths of the interactions with the

substrate. The xenon binding energy on Pt(111) is similar to the value on the (111) terraces of the stepped Pt(997) surface (approximately 260 meV). The pairwise attractive interaction of 11 meV is identical for both systems. Despite these similar parameters we have clearly shown that xenon desorption from the stepped surface obeys first-order compared to zero-order desorption on a flat surface, i.e., that a 2D gas-condensate equilibrium exists on Pt(111) during desorption, but not on Pt(997). This strong influence of the step structure on the terrace adsorption is interpreted as a breakdown of the 2D gas-condensed phase equilibrium, seen on the nominally flat surface, due to the finite size of the terrace widths on the stepped surface. Furthermore, indications of nonequilibrium effects during thermal desorption have been observed on the nominally flat surface which are absent on the stepped surface due to the finite-size-induced breakdown of the 2D gas-condensed phase equilibrium. These interpretations are supported by lattice-gas calculations analyzing the influence of terrace widths for two different stepped surfaces.

At low xenon coverages on Pt(997) we find xenon step decoration with a next-neighbor distance of 5.5 Å at 25 K and a repulsive pairwise lateral interaction of 16 meV during desorption. An additional slightly preferred adsorption site is populated before terrace adsorption occurs, which is interpreted as adsorption at the bottom of the step edge nucleating the terrace adsorption.

With the thermodynamics and kinetics on stepped surfaces so different from those on the corresponding flat surface one can conclude that from a study of adsorption on flat surfaces one can infer little about adsorption on stepped surfaces with terrace widths so small that only a fraction of adsorption sites are affected by the same nearest and next-nearest-neighbor environment as on the flat surface.

ACKNOWLEDGMENTS

This work was supported by the Deutsche Forschungsgemeinschaft through SFB 338 and by the German BMBF through Grant No. 05625WOA. This collaboration was made possible in large measure by financial support from the Humboldt foundation to H.J.K., who gratefully acknowledges the hospitality in Munich. The work at Dalhousie was supported by the Office of Naval Research and NSERC.

*Author to whom correspondence should be addressed. FAX: 49-89-2891-2338. Electronic address: widdra@physik.tu-muenchen.de

¹G. A. Somarjai, *Surf. Sci.* **299/300**, 849 (1994), and references therein.

²P. Kleban, in *Chemistry and Physics of Solid Surfaces V*, edited by R. Vanselow and R. Howe (Springer, Berlin, 1984).

³B. Poelsema, L. K. Verheij, and G. Comsa, *Phys. Rev. Lett.* **51**, 2410 (1983); *Surf. Sci.* **152/153**, 851 (1985).

⁴K. Kern, R. David, P. Zeppenfeld, and G. Comsa, *Solid State Commun.* **62**, 391 (1986).

⁵K. Kern, R. David, R. L. Palmer, and G. Comsa, *Phys. Rev. Lett.* **56**, 2823 (1986).

⁶K. Kern, *Phys. Rev. B* **35**, 8265 (1987).

⁷P. S. Weiss and D. M. Eigler, *Phys. Rev. Lett.* **69**, 2240 (1992).

⁸E. Hahn, H. Schief, V. Marsico, A. Fricke, and K. Kern, *Phys. Rev. Lett.* **72**, 3378 (1994).

⁹V. Marsico, M. Blanc, K. Kuhnke, and K. Kern, *Phys. Rev. Lett.* **78**, 94 (1997).

¹⁰S. Horch, P. Zeppenfeld, and G. Comsa, *Surf. Sci.* **331**, 908 (1995).

¹¹S. Horch, P. Zeppenfeld, and G. Comsa, *Appl. Phys. A: Solids Surf.* **60**, 147 (1995).

¹²C. T. Rettner, D. S. Bethune, and E. K. Schweizer, *J. Chem. Phys.* **92**, 1442 (1990).

¹³B. Poelsema, L. K. Verheij, and G. Comsa, *Surf. Sci.* **152-153**, 851 (1985).

¹⁴K. Wandelt, J. Hulse, and J. Küppers, *Surf. Sci.* **104**, 212 (1983).

¹⁵B. E. Nieuwenhuysh, D. T. Meijer, and W. M. H. Sachtler, *Phys. Status Solidi A* **24**, 115 (1974).

¹⁶H. R. Siddiqui, P. J. Chen, X. Guo, and J. T. Yates, Jr., *J. Chem. Phys.* **92**, 7690 (1990).

¹⁷P. Feulner and D. Menzel, *J. Vac. Sci. Technol.* **17**, 662 (1980).

- ¹⁸H. Schlichting and D. Menzel, *Rev. Sci. Instrum.* **64**, 2013 (1993); *Surf. Sci.* **272**, 27 (1992); **285**, 209 (1993).
- ¹⁹H. Schlichting, Ph.D. thesis, Technische Universität München, 1990; W. Frieß, Ph.D. thesis, Technische Universität München, 1994.
- ²⁰Strictly speaking, under equilibrium conditions all possible phases might be present with nonzero coverages: the 2D condensate in the first monolayer which acts as reservoir, the 2D gas phase on the bare metal, the 2D gas phase on the 2D condensate islands (i.e. 2D gas in the second layer), etc. However, in the range of unsaturated first layer as examined here, the latter coverage of the second layer will be very small due to the free energy differences.
- ²¹M. Potthoff, G. Hilgers, N. Müller, U. Heinzmann, L. Haunert, J. Braun, and G. Borstel, *Surf. Sci.* **322**, 193 (1995).
- ²²K. Kern, R. David, P. Zeppenfeld, and G. Comsa, *Surf. Sci.* **195**, 353 (1988).
- ²³The leading edge and isosteric analyses of the TPD spectra and the recalculation of the spectra were done with the ASTEK software package written by H. J. Kreuzer and S. H. Payne (available from Helix Science Applications, Box 49, Site 3, R.R. No. 5, Armdale N.S. B3L 4J5, Canada).
- ²⁴K. Kern, P. Zeppenfeld, R. David, R. L. Palmer, and G. Comsa, *Phys. Rev. Lett.* **57**, 3187 (1986).
- ²⁵K. Kern, P. Zeppenfeld, R. David, and G. Comsa, *J. Vac. Sci. Technol. A* **6**, 639 (1988).
- ²⁶For a review of lattice-gas models of adsorption and desorption see H. J. Kreuzer and S. H. Payne, in *Equilibrium and Dynamics of Gas Adsorption on Heterogeneous Solid Surfaces*, edited by W. Rudzinski, W. A. Steele, and G. Zgrablich (Elsevier, Amsterdam, 1997).
- ²⁷S. H. Payne and H. J. Kreuzer, *Surf. Sci.* **205**, 153 (1988); H. J. Kreuzer and S. H. Payne, *ibid.* **198**, 235 (1988).
- ²⁸S. H. Payne and H. J. Kreuzer, *Surf. Sci.* **285**, 153 (1988).
- ²⁹F. H. Ree and D. A. Chesnut, *J. Chem. Phys.* **45**, 3983 (1966); L. D. Roelofs and R. J. Bellon, *Surf. Sci.* **223**, 585 (1989); N. C. Bartelt, T. L. Einstein, and L. D. Roelofs, *Phys. Rev. B* **34**, 1616 (1986); P. A. Rikvold, K. Kaski, J. D. Gunton, and M. C. Yalabik, *ibid.* **29**, 6285 (1984); S. H. Payne, H. J. Kreuzer, and L. D. Roelofs, *Surf. Sci. Lett.* **259**, 781 (1991); S. H. Payne, Jun Zhang, and H. J. Kreuzer, *Surf. Sci.* **264**, 185 (1992).
- ³⁰See, e.g., T. L. Hill, *Statistical Mechanics* (McGraw-Hill, New York, 1956).
- ³¹We expect also contributions to the “rounding” of the TPD spectra from temperature gradients across the sampled crystal area. The fact that Pt(997), with a similar situation, does not show any such effects and that desorption from the second layer is more abrupt indicates that this contribution is small in our present cases.
- ³²K. Kern, R. David, R. L. Palmer, and G. Comsa, *Phys. Rev. Lett.* **56**, 620 (1986).
- ³³K. Kern, R. David, R. L. Palmer, and G. Comsa, *Surf. Sci. Lett.* **175**, L669 (1986).
- ³⁴J. M. Gottlieb and L. W. Bruch, *Phys. Rev. B* **44**, 5759 (1991).
- ³⁵L. W. Bruch, *Surf. Sci.* **125**, 194 (1983).
- ³⁶J. M. Gottlieb and L. W. Bruch, *Phys. Rev. B* **44**, 5750 (1991).
- ³⁷D. S. Bethune, J. A. Barker, and C. T. Rettner, *J. Chem. Phys.* **92**, 6847 (1990); C. R. Arumainayagam, R. J. Madix, M. C. McMaster, V. M. Suzawa, and J. C. Tully, *Surf. Sci.* **226**, 180 (1990); J. A. Barker, C. T. Rettner, and D. S. Bethune, *Chem. Phys. Lett.* **188**, 471 (1992); A. P. J. Jansen, *J. Chem. Phys.* **97**, 5205 (1992).
- ³⁸J. A. Barker, R. O. Watts, J. K. Lee, T. P. Schafer, and Y. T. Lee, *J. Chem. Phys.* **61**, 3081 (1974).
- ³⁹G. Schönhense, *Appl. Phys. A: Solids Surf.* **41**, 39 (1986).
- ⁴⁰E. Bertel, *Surf. Sci. Lett.* **367**, L61 (1996).
- ⁴¹J. E. Müller, *Phys. Rev. Lett.* **65**, 3021 (1990).